Original Article

Dosimetric impact of CT metal artifact reduction for spinal implants in stereotactic body radiotherapy planning

Bin Li[1#^], Jiexing Huang[1,2#], Junjie Ruan[1], Qinghe Peng[1], Sijuan Huang[1], Yunfei Li[1], Fanghua Li[1]

[1]State Key Laboratory of Oncology in South China, Collaborative Innovation Center for Cancer Medicine, Sun Yat-sen University Cancer Center, Guangzhou, China; [2]Department of Radiation Oncology, The First Affiliated Hospital, Sun Yat-sen University, Guangzhou, China

Contributions: (I) Conception and design: B Li, J Huang; (II) Administrative support: B Li; (III) Provision of study materials or patients: Q Peng, S Huang; (IV) Collection and assembly of data: B Li, J Huang, J Ruan, Y Li, F Li; (V) Data analysis and interpretation: J Huang, J Ruan; (VI) Manuscript writing: All authors; (VII) Final approval of manuscript: All authors.

[#]These authors contributed equally to this work.

Correspondence to: Bin Li, PhD. State Key Laboratory of Oncology in South China, Collaborative Innovation Center for Cancer Medicine, Sun Yat-sen University Cancer Center, 651 Dongfengdong Road, Yuexiu District, Guangzhou 510060, China. Email: libin1@sysucc.org.cn.

Background: Metal artifacts due to spinal implants may affect the accuracy of dose calculation for radiotherapy. However, the dosimetric impact of metal artifact reduction (MAR) for spinal implants in stereotactic body radiotherapy (SBRT) plans has not been well studied. The objective of this study was to evaluate the dosimetric impact of MAR in spinal SBRT planning with three clinically common dose calculation algorithms.

Methods: Gammex phantom and 10 patients' computed tomography (CT) images were studied to investigate the effects of titanium implants. A commercial orthopedic MAR algorithm was employed to reduce artifacts. Dose calculations for SBRT were conducted on both artifact-corrected and uncorrected images using three commercial algorithms [analytical anisotropic algorithm (AAA), Acuros XB (AXB), and Monte Carlo (MC)]. Dose discrepancies between artifact-corrected and uncorrected cases were appraised using a dose-volume histogram (DVH) and 3-dimensional (3D) gamma analysis with different distance to agreement (DTA) and dose difference criteria. The gamma agreement index (GAI) was denoted as G(ΔD, DTA). Statistical analysis of *t*-test was utilized to evaluate the dose differences of different algorithms.

Results: The phantom study demonstrated that titanium metal artifacts can be effectively reduced. The patient cases study showed that dose differences between the artifact-corrected and uncorrected datasets were small evaluated by gamma index and DVH. Gamma analysis found that even the strict criterion local G(1,1) had average values ≥93.9% for the three algorithms. For all DVH metrics, average differences did not exceed 0.7% in planning target volume (PTV) and 2.1% in planning risk volume of spinal cord (PRV-SC). Statistical analysis showed that the observed dose differences of MC method were significantly larger than those of AAA ($P<0.01$ for D98% of PTV and $P<0.001$ for D0.1cc of spinal cord) and AXB methods ($P<0.001$ for D98% and $P<0.0001$ for D0.1cc).

Conclusions: Dosimetric impact of artifacts caused by titanium implants is not significant in spinal SBRT planning, which indicates that dose calculation algorithms might not be very sensitive to CT number variation caused by titanium inserts.

Keywords: Dosimetric impact; metal artifacts reduction; stereotactic body radiotherapy (SBRT); spinal implant

^ ORCID: 0000-0002-2413-5175.

Submitted Apr 04, 2023. Accepted for publication Sep 14, 2023. Published online Oct 27, 2023.
doi: 10.21037/qims-23-442
View this article at: https://dx.doi.org/10.21037/qims-23-442

Introduction

Bone metastasis is one of the most common diseases for patients with advanced-stage cancers in breast, prostate, lung, and other sites. Spinal metastasis represents about 70% of all bone metastases and is the third most common site of metastasis (1,2). Metastatic spinal tumors can drastically reduce patients' quality of life as they frequently cause severe pain and are associated with spinal cord compression, pathologic fractures, hypercalcemia, immobility, and ultimate mortality (3). Conventional external beam radiotherapy (cEBRT) is a mainstay to reduce the risk of pathological fractures, neurological deficits, and pain (4). A study reported that around 60–80% of patients with painful spine metastases experienced pain relief after cEBRT, but the median duration of pain relief was only 4 months and only 25% of patients achieved complete remission (CR) (5). Stereotactic body radiotherapy (SBRT) is an effective approach for the management of spinal metastases (6). It uses intensity-modulated radiotherapy (IMRT) or volumetric-modulated arc therapy (VMAT), taking advantage of image-guided radiotherapy techniques, to produce highly tumor-conformal dose distributions with sharp dose fall-off to spare adjacent normal tissue. Typical SBRT delivery improves the radiotherapeutic index by precisely delivering the high radiation doses to the treatment area while keeping the spinal cord under a lower dose exposure to avoid severe toxicity (7,8). Several studies have reported the potential benefits of SBRT over cEBRT in relieving pain resulting from spinal metastases and achieving high rates of local tumor control with low-grade toxicity (9-11). In a recent randomized, controlled, multicenter, phase 2/3 trial, SBRT with a dose of 24 Gy in 2 daily fractions resulted in significantly higher rates of complete pain relief compared to cEBRT with a dose of 20 Gy in 5 daily fractions at 3 and 6 months post-treatment (12). A recent systematic review showed a satisfying result for the patients who received re-irradiation with SBRT after cEBRT, with 1-year local control rates ranging from 66% to 90% and the pain response rates ranging from 65% to 81% (13).

With the increasing utilization of SBRT in the management of spinal metastases, metal spinal implants adjacent to or within the treatment area are attracting attention because the sharp dose fall-off of SBRT requires a higher dose accuracy. The metal implants cause beam hardening, scattering effects, and photon starvation, which can lead to a reduced quality of computed tomography (CT) scans with the formation of dark streaks between the metals and bright streaks surrounding them. The resulting image degradation makes the delineation of the region of interest (ROI) a great challenge as well as affects negatively the tissue density estimate resulting in the potential of decrease in the dose calculation accuracy. In a single-patient study by Rong *et al.* (14), the metal artifacts caused by stainless steel spinal inserts were considered too severe, making conventional kV CT imaging unusable for treatment planning. Hence, megavoltage CT (MVCT) images were acquired to substantially reduce metal artifacts. Dose calculation on the MVCT images of the "cheese" phantom with different density plugs showed good agreement to measurement with a 3%/3 mm gamma criterion. In a phantom study, Son *et al.* (15) reported an average reduction of 2% in the dose calculation accuracy between titanium implants at the center of the phantom and a decrease in the dose calculation accuracy in the areas close to the surface of the titanium inserts. Spadea *et al.* (16) reported that underdosages of 20–25% were yielded in area around the high-Z metal implants in the uncorrected images whereas no significant discrepancies between the uncorrected and artifact-corrected images were observed for low-Z metal inserts. Nevertheless, comparatively few efforts have thoroughly investigated and quantified the clinical relevance of metal artifact reduction (MAR) method for different dose calculation algorithms in spinal SBRT planning.

Furthermore, metal artifacts due to spinal implants, including low-Hounsfield unit (HU) dark streaks and high-HU bright streaks, will lead to highly heterogeneous in structure. The heterogeneities of scattered radiation have to be considered because the dose distribution can be affected by changes in tissue composition. Dose calculation engines that precisely account for the heterogeneities contribute to a better insight into the radiation dose-response relationships between tumors and normal tissues. In general, different dose calculation algorithms provide different heterogeneity correction methods and hence they have different

sensitivities to metal artifacts. Some previous studies have investigated the impact of MAR on dose calculation for different algorithms (17-19). However, limitations exist: On the one hand, the compared dose calculation algorithms are not commonly used in clinical practice. On the other hand, some studies only experimented on phantoms without using clinical patient data. Analytical anisotropic algorithm (AAA), Acuros XB (AXB), and Monte Carlo (MC) are 3 commonly used commercial algorithms (20), and MC has been widely used as the gold standard method for dose calculation (21,22). However, few studies have sufficiently evaluated in actual patients the sensitivity of these three commonly clinical-used algorithms to metal artifacts.

The purpose of this work was to evaluate dosimetric effect of CT MAR in patient's spinal SBRT plan and the sensitivity of three commercial dose calculation algorithms (AAA, AXB, and MC) to the presence of titanium implants.

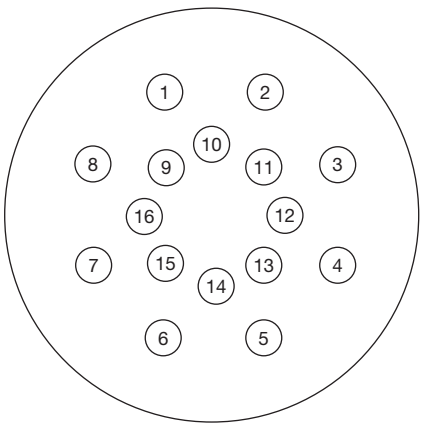

Figure 1 Layout of different inserted materials in the phantom.

Methods

Phantom study

Phantom images and MAR

A common quality assurance (QA) phantom in radiotherapy was used to evaluate the image quality and dosimetric impact of MAR for planning dose calculation. This Gammex 467 tissue characterization phantom (Gammex-RMI, Middleton, WI, USA) was made of a solid water disc of 33 cm diameter, comparable in size to the average pelvis. A matrix with 16 holes of 2.8 cm diameter in the disc accommodates interchangeable rods of different tissue and water substitutes, as shown in *Figure 1*. The physical characteristics of these substitutes are listed in *Table 1*. A Philips Brilliance big bore CT scanner (Philips Healthcare, Amsterdam, Netherlands) was used to scan the phantom with 3 mm slice thickness at 140 kVp. A planning target volume (PTV) was contoured for the SBRT planning. The target extended 1.8 cm in the superior-inferior direction to

Table 1 Physical characteristics of the Gammex phantom inserts

Label index	Material	Physical density (g/cm^3)	Electron density relative to water
1	AP6 adipose	0.945	0.928
2	LN-450 lung	0.47	0.456
3	Cortical bone	1.824	1.696
4	BR-12 breast	0.977	0.954
5, 11, 14	Solid water	1.017	0.988
6	CB2-30%	1.333	1.278
7	CB2-50%	1.561	1.471
8	LN-300 lung	0.28	0.275
9	B200 bone	1.150	1.102
10	Water insert	1	1.000
12	LV1 liver	1.095	1.063
13, 15	Titanium	4.54	3.730
16	Inner bone	1.133	1.086

The label indexes correspond to the labels shown in *Figure 1*.

include virtually all volumes of the titanium rods and most of the artifacts. The area next to the target was selected and delineated as pseudo organ at risk (p-OAR).

At present, a commercial artifact reduction algorithm is a feasible strategy to solve the problem of metal artifacts in CT images. In most MAR algorithms, the damaged data due to the presence of metals is first detected and treated as missing data. The data is then restored by various interpolations of different algorithm designs, and subsequently reconstructed to final CT images. The orthopedic metal artifact reduction (OMAR) iterative algorithm (23), equipped on a Philips CT scanner, was employed to suppress the artifacts caused by titanium rods in this study. In order to obtain a ground truth image without metal artifacts, two solid water rods were used to replace the titanium rods in the phantom before the phantom was scanned. Subsequently, we assigned titanium density of 4.5 g/cm^3 to the volumes of the two solid water rods.

Treatment planning and dose calculation

A VMAT plan that followed the SBRT treatment planning guidelines (24) was designed on Monaco treatment planning system (TPS) (Elekta AB, Stockholm, Sweden). The plan was optimized on the ground truth image, and then duplicated to the uncorrected and artifact-corrected images, respectively, with identical beam parameters. Dose calculation was then carried out on all three image sets using MC algorithm with dose grid of 1.8 mm and dose reporting mode set as dose-to-medium. The MC algorithm is more accurate than other dose calculation algorithms and hence it was chosen for dosimetric evaluation of this phantom study. The electron density of the area where the HU value exceeded 2,300 was set to 3.73 according to the titanium's physical properties.

Data analysis

SNC Patient (Sun Nuclear Inc, Melbourne, FL, USA) was used to evaluate the planar dose distribution differences of the uncorrected/corrected CT images from the reference CT images. The dose coverage difference (corrected *vs.* uncorrected) was scored by using the 2-dimensional (2D) gamma (γ) index using both global and local difference setting. The dose threshold was set to a 10% cutoff value of prescription dose to exclude low-dose areas. Various threshold criteria were used: dose difference (ΔD) = 1%, 2%, and 3%, distance to agreement (DTA) = 1, 2, and 3 mm. We obtained a total of 3 gamma agreement index (GAI) values G(ΔD, DTA): G(1,1), G(2,2), and G(3,3).

We evaluated the dose distribution differences for the various structures by comparing typical clinical dose-volume histogram (DVH) metrics. The DVH analysis of PTV included D98% (% of prescription dose covering 98% of the volume), D50%, D2%, D2cc (the percentage of the prescription dose received by 2 cc of the volume), and Dmean (mean dose). For the p-OAR, D0.1cc, D1cc, D3cc, and Dmean were compared.

Patient study

Patient data and MAR

A total of 10 patients with spine metastasis were randomly selected from 2019 to 2021 in Sun Yat-sen University Cancer Center for this study. The study was conducted in accordance with the Declaration of Helsinki (as revised in 2013). The study was approved by the Ethics Committee of Sun Yat-sen University Cancer Center (No. B2022-498-01) and the requirement for individual consent for this retrospective analysis was waived. Radiation treatments were administered after surgical resection of the tumor and insertion of titanium implants for stabilizing the spinal column. The implants included a spinal fusion cage and three screws that are partially contained within the PTV. The artifacts were mainly manifested as dark streaks that overlapped heavily with normal tissue in the central area. All the CT images of patients were also acquired on a Philips Brilliance Big Bore CT scanner with 3 mm slice thickness at 140 kVp. OMAR was also used to reduce the artifacts caused by the titanium inserts. The radiation treatment included one plan using IMRT and nine plans using the VMAT technique.

Treatment planning and dose calculation

We designed five SBRT plans in the Eclipse TPS (Version 15.5; Varian Medical Systems, Palo Alto, CA, USA). All plan optimizations were based on the uncorrected images. Calculation of dose distribution was performed on both the uncorrected and artifact-corrected images by using the AAA algorithm (Version 15.5.12) with heterogeneity correction. Subsequently, the AXB algorithm (Version 15.5.12) with dose reporting mode and dose-to-medium setting was used to recalculate all these plans.

Another five SBRT plans were designed in the Monaco TPS (Version 5.11.03; Elekta AB). The MC algorithm (Version 1.6) equipped in the Monaco TPS was employed to perform the dose calculation. Previous studies have

shown that this MC calculation can provide an accurate dose distribution in both homogeneous and heterogeneous media (25-27). Dose-to-medium was considered for calculation.

The SBRT delivery technique included IMRT and VMAT. Grid size was set to be 1.8 mm for all calculations. Note that, numbers of pixels with a CT value corresponding to a mass density value above 3.0 g/cc (2,435 HU) exceeded the tolerance limit defined in the AXB calculation options. We collected all high-density pixels and assigned titanium alloy material for them. All dose calculations were conducted by using a corrected CT density curve where the titanium density was 4.5 g/cm^3.

Data analysis

3D Slicer (Version 4.11.20210226; https://www.slicer.org/) was used for evaluation in these patient cases. Dose coverage difference was scored by using the 3D γ index with both global and local normalization. The DVH analysis of PTV included D98%, D50%, D2%, and Dmean. For the planning risk volume of spinal cord (PRV-SC), which is obtained by extending 5 mm in each direction of the spinal cord, indicators recommended by stereotactic ablative body radiotherapy (SABR) consortium guidelines of UK (28) are quantified which included mean dose and maximum significant doses such as D0.1cc and D1cc. Statistical analysis was conducted using GraphPad Prism 8.0 (GraphPad Software, San Diego, CA, USA). Differences between groups were analyzed by *t*-test. The difference was considered statistically significant if $P<0.05$.

Results

Phantom study

The representative slices of the uncorrected, artifact-corrected, and reference CT images are shown in *Figure 2A-2C*. CT numbers for 1 horizontal profile connecting the two titanium inserts and the other vertical profile passing through the middle of the line connecting the two titanium inserts are shown in *Figure 2D,2E*. The specific locations of the profiles are indicated in the reference image in *Figure 2C*. The CT numbers for the uncorrected images deviated significantly from those of the reference image, whereas the CT numbers for the corrected images were close to those of the reference image, indicating that the CT numbers were prominently retrieved in the heavily shaded area between the two titanium inserts by using OMAR. However, additional artifacts were introduced, as indicated by the yellow arrows in *Figure 2B*. *Figure 2F-2I* presents dose profiles and dose differences from the reference dose distribution. A better agreement is achieved between the dose distributions calculated from OMAR-corrected images and the reference images, compared with that of uncorrected images.

Table 2 presents the gamma analysis results within 10% isodose volume, quantifying the distribution of doses calculated on corrected and uncorrected images versus ground truth image. OMAR-Org denotes the comparison of uncorrected and OMAR-corrected datasets. Ref-Org represents the comparison of uncorrected and reference datasets. Ref-OMAR indicates the comparison of OMAR and reference dataset. The calculated dose distribution on the corrected images is consistent with the reference dose distribution. With global normalization, all passing rates exceeded 94%. With local normalization, passing rates were over 92%, except for the G(1,1) for OMAR-Org and Ref-Org, which were 88.7% and 84.9%, respectively. *Table 3* presents the DVH analysis results. In terms of D0.1cc, D1cc, and D3cc for p-OAR, OMAR-Org and Ref-Org showed high differences which were more than 4% due to large sizes of titanium inserts. The differences between OMAR and the reference dataset did not exceed 1% for all parameters, indicating that OMAR can achieve satisfactory reduction of metal artifacts and it can be used to deal with the metal artifacts in patients' images.

Patient study

In *Figure 3*, a representative slice of the uncorrected and artifacts-corrected CT, the dose difference and DVH from a representative patient case are shown. The minimum and maximum values of dose difference were approximately within ±30 cGy (±1%). Differences ranging from 26 to 30 cGy (0.88–1%) are mainly distributed around the titanium inserts. The dose differences in other regions were lower than 26.6 cGy (0.88%) and randomly distributed, which may be related to the probabilistic process used in MC dose calculation. No significant difference was observed between the corrected and uncorrected datasets from the DVH of this patient case. CT numbers for one horizontal profile connecting the two titanium inserts and the other vertical profile passing through the middle of the line connecting the two titanium inserts are shown in *Figure 4A,4B*. The specific locations of the profiles are indicated in the original image in *Figure 3*. *Figure 4C-4F*

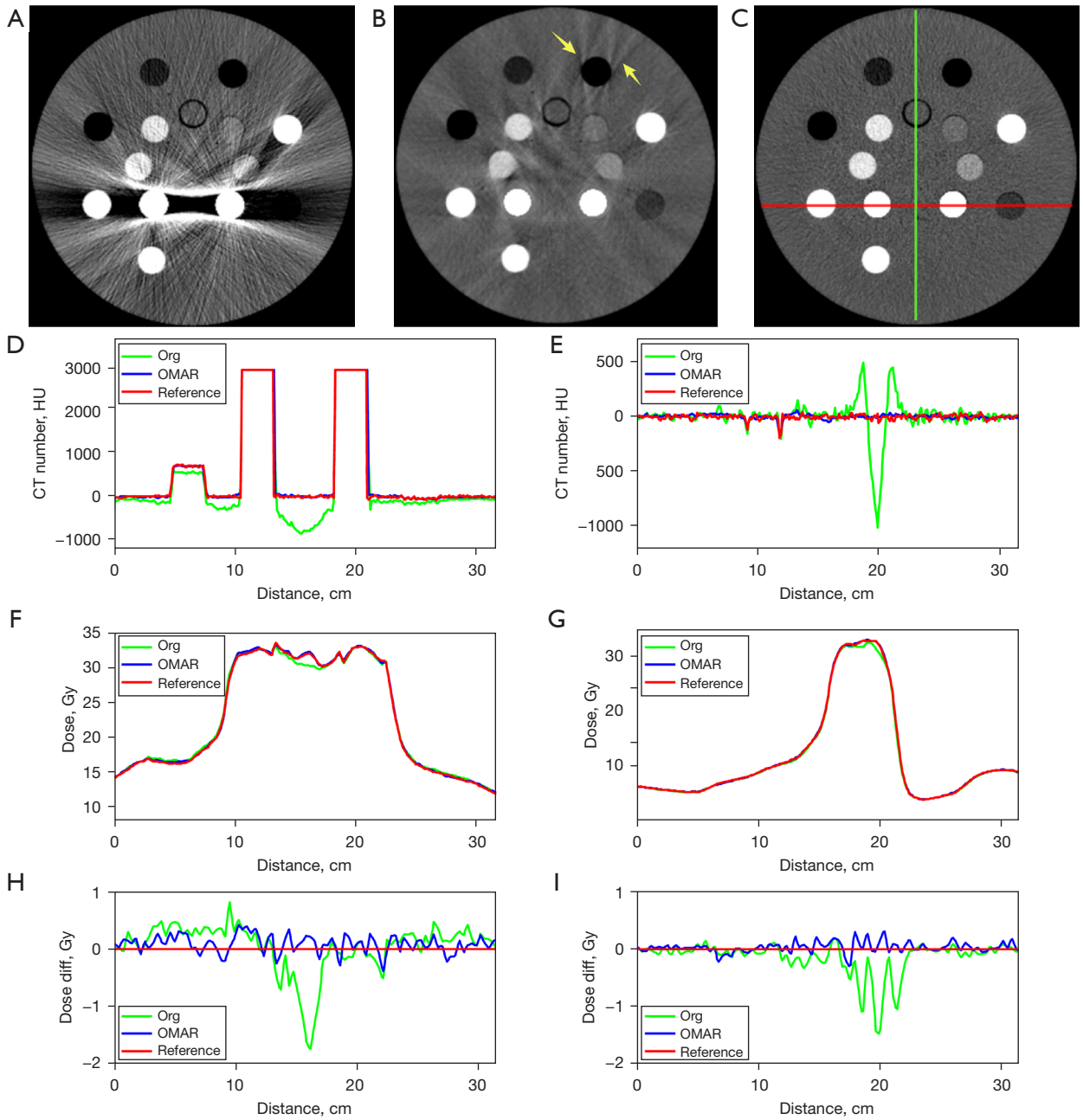

Figure 2 Illustration of phantom study and profile comparison. The uncorrected image (A), artifact-corrected image (B), and reference CT image (C). The arrows indicate the additional artifacts introduced by OMAR algorithm. (D-G) The HU and dose profile through the region of the most significant artifacts indicated by the red dashed line on the image, respectively. (D) Horizon profile (left to right) and (E) vertical profile (up to down) of CT number along the two lines indicated in the reference image. (F,G) The corresponding dose profiles. (H,I) The corresponding dose difference plots. CT, computed tomography; OMAR, orthopedic metal artifact reduction; HU, Hounsfield units.

Table 2 Gamma analysis results

Group comparison	Global			Local		
	G(1,1)	G(2,2)	G(3,3)	G(1,1)	G(2,2)	G(3,3)
OMAR-Org	96.2%	99.3%	99.8%	88.7%	99.6%	99.9%
Ref-Org	94.7%	98.9%	99.7%	84.9%	98.5%	99.8%
Ref-OMAR	99.0%	99.9%	100.0%	92.3%	99.6%	99.9%

OMAR, orthopedic metal artifact reduction; Org, original.

Table 3 A summary of results for all dosimetric parameters analyzed

Group comparison	PTV				p-OAR			
	Dmean	D98%	D2%	D50%	Dmean	D0.1cc	D1cc	D3cc
OMAR-Org	1.28%	3.62%	0.24%	1.06%	2.27%	4.51%	4.63%	4.06%
Ref-Org	1.68%	3.80%	0.66%	1.49%	2.63%	4.46%	4.86%	4.21%
Ref-OMAR	0.39%	0.17%	0.42%	0.42%	0.36%	–0.04%	0.22%	0.15%

PTV, planning target volume; p-OAR, pseudo organ at risk; OMAR, orthopedic metal artifact reduction; Org, original.

presents dose profiles and dose differences between corrected and uncorrected datasets. Although significant shadows caused a noticeable decrease in the representative HU values, dose differences between corrected and uncorrected datasets did not exceed 1 Gy.

The graphic results of the 3D gamma analysis between uncorrected and artifact-corrected datasets for all algorithms are presented in *Figure 5A*,*5B*. With both global and local normalization, the AAA method yielded the values of both G(2,2) and G(3,3) equal to 100% for all patients. AXB was yielded a minimum G(2,2) value of 98.2% with global normalization and 95.4% with local normalization. MC yielded minimum G(2,2) values with global and local normalization of 97.9% and 97.7%, respectively. The highest passing rates of G(1,1) were observed to be 99.9%±0.1% with global normalization and 99.5%±0.2% with local normalization in the AAA algorithm. In contrast, AXB yielded values with an average of 96.0%±3.7% with global normalization and 95.0%±6.6% with local normalization, respectively. MC yielded values with an average of 94.5%±2.6% and 93.9%±1.3% with global and local normalization, respectively. Furthermore, we found that the passing rates of AAA are significantly higher than that of AXB (global: P=0.003; local: P=0.03) and MC (global: P<0.001; local: P=0.001), respectively.

Figure 5C,*5D* present a summary of the absolute dose differences between uncorrected and corrected datasets comparison of DVH obtained from the dose distributions of calculated with AAA, AXB, and MC. Due to the variety of prescriptions, all data were shown as percentages. Minor discrepancies were seen between uncorrected and artifact-suppressed datasets for all algorithms. In all cases for PTV, average differences did not exceed 0.7%, for PRV-SC these reached 2.1%. Moreover, in terms of D0.1cc, D98%, and D2%, the observed dose differences of the MC method were statistically significantly larger than those of the AAA (P<0.01 for D98% and P<0.001 for D0.1cc) and AXB (P<0.001 for D98% and P<0.0001 for D0.1cc) methods, yet no significance was determined in terms of Dmean, D50%, and D1cc.

Discussion

In this work, we investigated the dosimetric impact of MAR for spinal implants in SRBT. Some previous studies have evaluated the dosimetric impact of metal artifacts on dose calculation algorithms. Using MC as a reference, Wang *et al.* (17) evaluated the accuracy of an analytical (Pinnacle3) dose calculation in the presence of titanium rod in water. In a study by Shen *et al.* (18), dosimetric effects of OMAR in different metal locations and dose calculation algorithms were evaluated. Furthermore, the dosimetric accuracy of AAA and AXB for small radiation fields incident on phantoms of various metals was investigated by Akdeniz

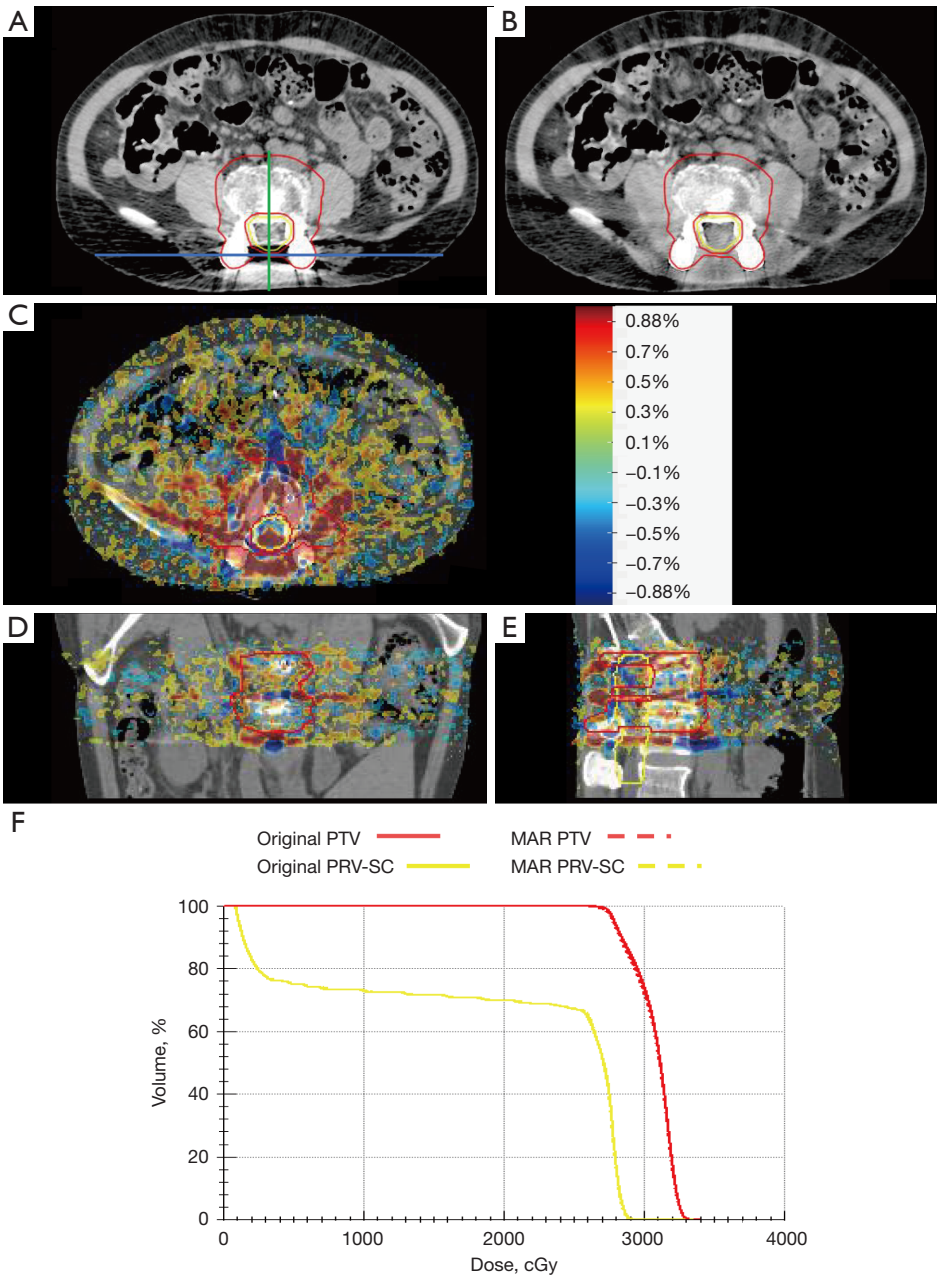

Figure 3 Illustration of one patient's images and planning dose comparison of the uncorrected and OMAR-corrected datasets. (A) Uncorrected image; (B) corrected image; (C) transversal view; (D) coronal view; (E) sagittal view; (F) DVH. PTV, planning target volume; MAR, metal artifact reduction; PRV-SC, planning risk volume of spinal cord; DVH, dose-volume histogram; OMAR, orthopedic metal artifact reduction.

et al. (19). However, certain limitations remain: (I) using non-clinically common algorithms; (II) only analyzing phantoms without clinical patient data. In order to more closely match the actual clinical conditions, this work makes two contributions: (I) quantifying dosimetric effect of CT MAR in spinal SBRT plan using both phantom and patient experiments on three mainstream commercial dose calculation algorithms (AAA, AXB, and MC); (II) assessing the sensitivity of three commercial dose calculation algorithms to titanium implants.

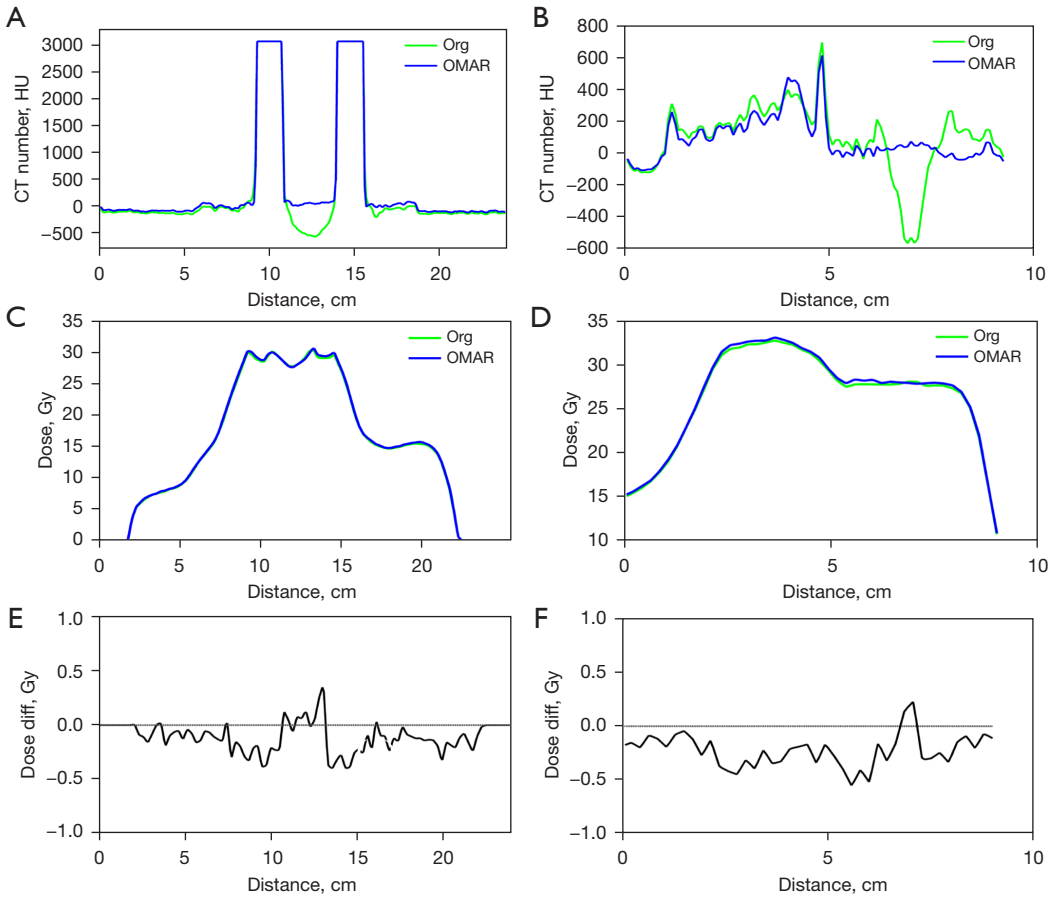

Figure 4 CT number and planning dose comparison. (A) Horizon profile (left to right) and (B) vertical profile (up to down) of CT number along the two lines indicated in the original image in *Figure 3A*. (C,D) The corresponding dose profiles. (E,F) The corresponding dose difference plots. CT, computed tomography; Org, original; OMAR, orthopedic metal artifact reduction.

The results of the phantom study showed that OMAR can achieve satisfactory reduction of metal artifacts. Analysis of gamma index and DVH in patients revealed small dosimetric discrepancies between uncorrected and artifact-corrected datasets for all dose calculation algorithms. With the thresholds of 3%/3 mm and 2%/2 mm, all dose calculation algorithms yielded high gamma passing rates exceeding 95.4%. Even using the stricter criteria of 1%/1 mm, passing rates with global normalization still exceeded 90%. Note that relatively lower local gamma passing rates were found in two cases (81.8% for AXB, 88.8% for MC), due to bigger dose discrepancy in the steep dose gradient region. In the case of AAA and AXB methods, the maximum difference of each evaluation index of DVH is less than 0.6%, except for an AXB case where the D50% difference in PTV reaches 0.8%. For the MC method, the median of D0.1cc was 2.19% and the maximum of D0.1cc reached 3.3%. The average of Dmean and D1cc were 0.74%±0.34% and 0.87%±0.93%, respectively. The small dosimetric differences might be accounted for in the following aspects. Firstly, titanium is a relatively low atomic number (Z) metal. Spadea *et al.* (16) found that low-Z metallic materials, such as titanium inserts, have little perturbation in the precision of the dose distribution near the metal attachment in IMRT. Secondly, in case of the same type of metal, the degree of artifacts also relies on the size of inserts with larger implants yielding more severe artifacts. In the phantom study, even for two titanium rods with a diameter of 2.5 cm, the maximum dose error was a 4.86% decrease in D1cc in the p-OAR. The diameter of titanium implants in the spine is generally not large enough to produce artifacts causing large dose perturbations. Thirdly, the estimation errors depend on the number of beams applied in a plan, the dosimetric effect might

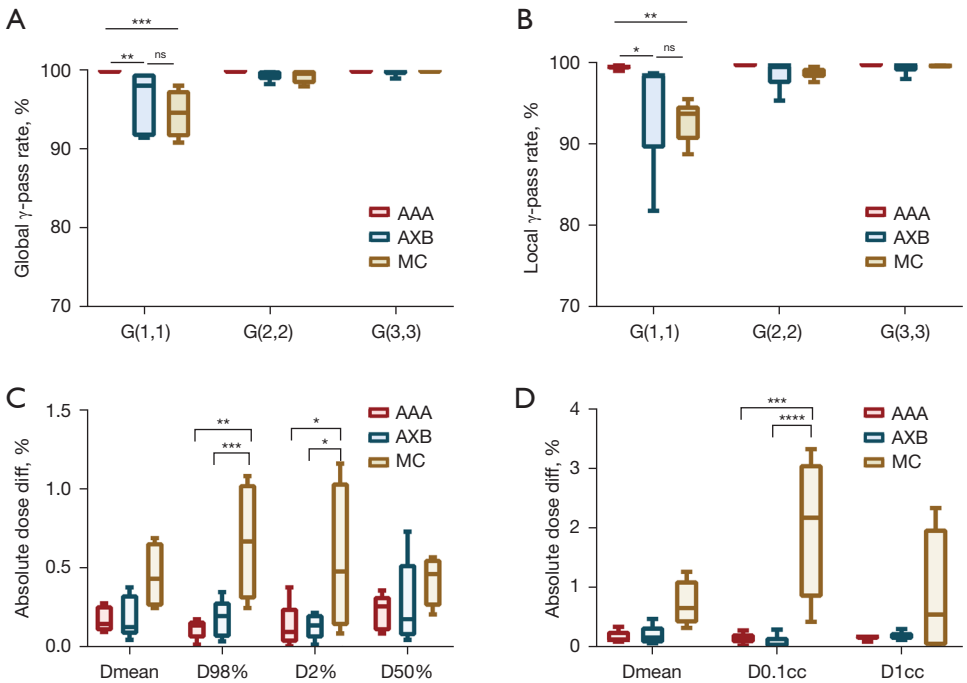

Figure 5 Statistical results of 3D gamma analysis and dose difference. (A,B) The 3D gamma analysis between uncorrected and artifact-suppressed datasets for all algorithms using global and local difference setting, respectively. (C,D) The dose difference between the uncorrected datasets and artifact-suppressed datasets in PTV and planning risk volume of spinal cord for all algorithms. The lines in the boxplot denote the median. Differences between groups were analyzed by *t*-test. P<0.05 was considered statistically significant. *, P<0.05; **, P<0.01; ***, P<0.001; ****, P<0.0001. PTV, planning target volume; AAA, analytical anisotropic algorithm; AXB, Acuros XB; MC, Monte Carlo; 3D, 3-dimensional.

be reduced by the increasing number of beams (29). In contrast, Brożyna *et al.* (30) detected an overdose of 109% due to back scatter in a single-beam study. In this study, the plans employed the VMAT technique or IMRT with seven beams, where the doses were delivered from multiple directions, resulting in averaging of the artifact-induced dose inhomogeneity.

In terms of D98% and D2% for PTV, and D0.1cc for PRV-SC, the observed differences between MC and AAA, as well as between MC and AXB, showed statistical significance. MC was found to have the highest sensitivity to artifacts caused by titanium implants compared with the AAA and AXB methods, because it explicitly models the interaction of radiation within and around the inhomogeneous media, resulting in accurate dose estimates. Currently, MC has been widely used as the gold standard method for dose calculation (22,31). Note that MC in the Monaco system would not allow the designation of titanium and this might cause the inaccuracy dose around spinal implants. On the other hand, the AAA method showed the lowest sensitivity to artifacts caused by titanium implants, with the maximum difference of each evaluation index of DVH not exceeding 0.5%. This is probably due to the fact that AAA is developed based on the superposition/convolution method, where approximation exists in the dose calculation process. In AAA, dose is calculated by superposition of the dose kernels of the primary and scattering components obtained by MC, and all model parameters were calculated in water equivalent medium. Tissue inhomogeneity corrections were performed in only four lateral directions and were approximated. It has been reported that the dose distribution in AAA deviates from the measured values in and around the non-uniform medium (32,33). Although the same photon beam source model is shared by the AXB and AAA, differences exist in radiation transport and energy deposition within volumes. AXB improves the accuracy of dose calculation by solving the linear Boltzmann transport equation to calculate the particle fluence based on specific material and energy interactions. Obviously, it is configured with dose-to-medium reporting

mode, which is more common than dose-to-water mode.

One limitation of this work is that no actual measurement experiments were conducted, because the main scope of this study was to evaluate the dosimetric impact of MAR on dose calculation algorithms in spinal SBRT planning. In the future, we would design anthropomorphic phantoms to validate the dose calculation accuracy by comparing different calculation algorithms with measured dose distribution. Another limitation is that AAA/AXB and MC were not performed in the same plan. Ideally, a rigorous evaluation is calculating the same plan in different dose calculation algorithms to compare their sensitivity to spinal implant artifacts. In our institution, there is no same machine modeled in both Monaco and Eclipse systems. This makes the same plan calculated in 1 TPS unable to be recalculated in another TPS. In a feasible way, we used statistical analysis of multiple cohorts to compare the sensitivity of different dose calculation algorithms to the titanium artifacts.

Conclusions

In this study, we evaluated the dosimetric impact of MAR for spinal implants in SBRT plans. From the perspective of dose calculation accuracy, CT image artifacts caused by titanium implants have little effect on dose distribution of spinal SBRT plans. Moreover, the MC algorithm has higher sensitivity to metal artifacts compared to AAA and AXB, indicating that MC is preferable for dose calculation in spinal SBRT planning.

Acknowledgments

Funding: This work was partially supported by the Guangdong Basic and Applied Basic Research Foundation (No. 2020A1515110352) and the Special Scientific Research Fund for Medical Physics & Technology of Guangdong Biomedical Engineering Society (No. 2022YXWL0101).

Footnote

Conflicts of Interest: All authors have completed the ICMJE uniform disclosure form (available at https://qims.amegroups.com/article/view/10.21037/qims-23-442/coif). The authors have no conflicts of interest to declare.

Ethical Statement: The authors are accountable for all aspects of the work in ensuring that questions related to the accuracy or integrity of any part of the work are appropriately investigated and resolved. The study was conducted in accordance with the Declaration of Helsinki (as revised in 2013). The study was approved by the Ethics Committee of Sun Yat-sen University Cancer Center (No. B2022-498-01) and the requirement for individual consent for this retrospective analysis was waived.

References

1. Randall RL. A promise to our patients with metastatic bone disease. Ann Surg Oncol 2014;21:4049-50.
2. Quinn RH, Randall RL, Benevenia J, Berven SH, Raskin KA. Contemporary management of metastatic bone disease: tips and tools of the trade for general practitioners. J Bone Joint Surg Am 2013;95:1887-95.
3. Krzeszinski JY, Wan Y. New therapeutic targets for cancer bone metastasis. Trends Pharmacol Sci 2015;36:360-73.
4. Lutz S, Balboni T, Jones J, Lo S, Petit J, Rich SE, Wong R, Hahn C. Palliative radiation therapy for bone metastases: Update of an ASTRO Evidence-Based Guideline. Pract Radiat Oncol 2017;7:4-12.
5. Rades D, Lange M, Veninga T, Stalpers LJ, Bajrovic A, Adamietz IA, Rudat V, Schild SE. Final results of a prospective study comparing the local control of short-course and long-course radiotherapy for metastatic spinal cord compression. Int J Radiat Oncol Biol Phys 2011;79:524-30.
6. Vellayappan BA, Chao ST, Foote M, Guckenberger M, Redmond KJ, Chang EL, Mayr NA, Sahgal A, Lo SS. The evolution and rise of stereotactic body radiotherapy (SBRT) for spinal metastases. Expert Rev Anticancer Ther 2018;18:887-900.
7. Sahgal A, Roberge D, Schellenberg D, Purdie TG, Swaminath A, Pantarotto J, Filion E, Gabos Z, Butler J, Letourneau D, Masucci GL, Mulroy L, Bezjak A, Dawson LA, Parliament M; . The Canadian Association of Radiation Oncology scope of practice guidelines for lung,

liver and spine stereotactic body radiotherapy. Clin Oncol (R Coll Radiol) 2012;24:629-39.
8. Seung SK, Larson DA, Galvin JM, Mehta MP, Potters L, Schultz CJ, Yajnik SV, Hartford AC, Rosenthal SA. American College of Radiology (ACR) and American Society for Radiation Oncology (ASTRO) Practice Guideline for the Performance of Stereotactic Radiosurgery (SRS). Am J Clin Oncol 2013;36:310-5.
9. Chang JH, Shin JH, Yamada YJ, Mesfin A, Fehlings MG, Rhines LD, Sahgal A. Stereotactic Body Radiotherapy for Spinal Metastases: What are the Risks and How Do We Minimize Them? Spine (Phila Pa 1976) 2016;41 Suppl 20:S238-45.
10. Spencer KL, van der Velden JM, Wong E, Seravalli E, Sahgal A, Chow E, Verlaan JJ, Verkooijen HM, van der Linden YM. Systematic Review of the Role of Stereotactic Radiotherapy for Bone Metastases. J Natl Cancer Inst 2019;111:1023-32.
11. Glicksman RM, Tjong MC, Neves-Junior WFP, Spratt DE, Chua KLM, Mansouri A, Chua MLK, Berlin A, Winter JD, Dahele M, Slotman BJ, Bilsky M, Shultz DB, Maldaun M, Szerlip N, Lo SS, Yamada Y, Vera-Badillo FE, Marta GN, Moraes FY. Stereotactic Ablative Radiotherapy for the Management of Spinal Metastases: A Review. JAMA Oncol 2020;6:567-77.
12. Sahgal A, Myrehaug SD, Siva S, Masucci GL, Maralani PJ, Brundage M, et al. Stereotactic body radiotherapy versus conventional external beam radiotherapy in patients with painful spinal metastases: an open-label, multicentre, randomised, controlled, phase 2/3 trial. Lancet Oncol 2021;22:1023-33.
13. Myrehaug S, Soliman H, Tseng C, Heyn C, Sahgal A. Re-irradiation of Vertebral Body Metastases: Treatment in the Radiosurgery Era. Clin Oncol (R Coll Radiol) 2018;30:85-92.
14. Rong Y, Yadav P, Paliwal B, Shang L, Welsh JS. A planning study for palliative spine treatment using StatRT and megavoltage CT simulation. J Appl Clin Med Phys 2010;12:3348.
15. Son SH, Kang YN, Ryu MR. The effect of metallic implants on radiation therapy in spinal tumor patients with metallic spinal implants. Med Dosim 2012;37:98-107.
16. Spadea MF, Verburg JM, Baroni G, Seco J. The impact of low-Z and high-Z metal implants in IMRT: a Monte Carlo study of dose inaccuracies in commercial dose algorithms. Med Phys 2014;41:011702.
17. Wang X, Yang JN, Li X, Tailor R, Vassilliev O, Brown P, Rhines L, Chang E. Effect of spine hardware on small spinal stereotactic radiosurgery dosimetry. Phys Med Biol 2013;58:6733-47.
18. Shen ZL, Xia P, Klahr P, Djemil T. Dosimetric impact of orthopedic metal artifact reduction (O-MAR) on Spine SBRT patients. J Appl Clin Med Phys 2015;16:106-16.
19. Akdeniz Y, Yegingil I, Yegingil Z. Effects of metal implants and a metal artifact reduction tool on calculation accuracy of AAA and Acuros XB algorithms in small fields. Med Phys 2019;46:5326-35.
20. Chaikh A, Balosso J. Quantitative comparison of dose distribution in radiotherapy plans using 2D gamma maps and X-ray computed tomography. Quant Imaging Med Surg 2016;6:243-9.
21. Zhang B, Liu X, Chen L, Zhu J. Convolution neural network toward Monte Carlo photon dose calculation in radiation therapy. Med Phys 2022;49:1248-61.
22. Park H, Paganetti H, Schuemann J, Jia X, Min CH. Monte Carlo methods for device simulations in radiation therapy. Phys Med Biol 2021;66:10.1088/1361-6560/ac1d1f.
23. Li H, Noel C, Chen H, Harold Li H, Low D, Moore K, Klahr P, Michalski J, Gay HA, Thorstad W, Mutic S. Clinical evaluation of a commercial orthopedic metal artifact reduction tool for CT simulations in radiation therapy. Med Phys 2012;39:7507-17.
24. Wilke L, Andratschke N, Blanck O, Brunner TB, Combs SE, Grosu AL, Moustakis C, Schmitt D, Baus WW, Guckenberger M. ICRU report 91 on prescribing, recording, and reporting of stereotactic treatments with small photon beams : Statement from the DEGRO/DGMP working group stereotactic radiotherapy and radiosurgery. Strahlenther Onkol 2019;195:193-8.
25. Fragoso M, Wen N, Kumar S, Liu D, Ryu S, Movsas B, Munther A, Chetty IJ. Dosimetric verification and clinical evaluation of a new commercially available Monte Carlo-based dose algorithm for application in stereotactic body radiation therapy (SBRT) treatment planning. Phys Med Biol 2010;55:4445-64.
26. Petoukhova AL, van Wingerden K, Wiggenraad RG, van de Vaart PJ, van Egmond J, Franken EM, van Santvoort JP. Verification measurements and clinical evaluation of the iPlan RT Monte Carlo dose algorithm for 6 MV photon energy. Phys Med Biol 2010;55:4601-14.
27. Zhuang T, Djemil T, Qi P, Magnelli A, Stephans K, Videtic G, Xia P. Dose calculation differences between Monte Carlo and pencil beam depend on the tumor locations and volumes for lung stereotactic body radiation therapy. J Appl Clin Med Phys 2013;14:4011.
28. UK SABR Consortium. Stereotactic Ablative Radiation

Therapy (SABR): a resource. v6.1, January 2019. [accessed 20 July 2019]. Available online: https://www.sabr.org.uk/wp-content/uploads/2019/04/SABRconsortium-guidelines-2019-v6.1.0.pdf
29. Giantsoudi D, De Man B, Verburg J, Trofimov A, Jin Y, Wang G, Gjesteby L, Paganetti H. Metal artifacts in computed tomography for radiation therapy planning: dosimetric effects and impact of metal artifact reduction. Phys Med Biol 2017;62:R49-80.
30. Brożyna B, Chełmiński K, Bulski W, Giżyńska M, Grochowska P, Walewska A, Zalewska M, Kawecki A, Krajewski R. Dosimetry of dose distributions in radiotherapy of patients with surgical implants. Radiation Physics and Chemistry 2014;104:170-4.
31. Keal J, Santos A, Penfold S, Douglass M. Radiation dose calculation in 3D heterogeneous media using artificial neural networks. Med Phys 2021;48:2637-45.
32. Yang B, Liu Y, Chen Z, Wang Z, Zhou Q, Qiu J. Tissues margin-based analytical anisotropic algorithm boosting method via deep learning attention mechanism with cervical cancer. Int J Comput Assist Radiol Surg 2023;18:953-9.
33. Abdullah C, Farag H, El-Sheshtawy W, Aboelenein H, Guirguis OW. Clinical impact of anisotropic analytical algorithm and Acuros XB dose calculation algorithms for intensity modulated radiation therapy in lung cancer patients. J Xray Sci Technol 2021;29:1019-31.

Cite this article as: Li B, Huang J, Ruan J, Peng Q, Huang S, Li Y, Li F. Dosimetric impact of CT metal artifact reduction for spinal implants in stereotactic body radiotherapy planning. Quant Imaging Med Surg 2023;13(12):8290-8302. doi: 10.21037/qims-23-442

